Comparative Vibrational Spectroscopic Studies

Bull. Korean Chem. Soc., Vol. 10, No. 1, 1989 39

lishing Co., New York, 1950.

5. L. Onsager, *J. Am. Chem. Soc.,* **58**, 1486 (1936).

6. G. Oster, *J. Am. Chem. Soc.,* **68**, 2036 (1946).

7. S. Nagakura and H. Baba, *J. Am. Chem. Soc.,* **74**, 5693 (1952).

8. G. Oster, *J. Am. Chem. Soc.,* **66**, 948 (1944).

9. A.M.F. Barton, *Chem. Rev.,* **75**, 731 (1975).

10. A. Purkayastha and J. Walkley, *Can. J. Chem.,* **50**, 834 (1972).

11. R. F. Blanks and J. M. Pausnitz, *Ind. Eng. Chem. Fundam.,* **3**, 1 (1964).

12. C. V. Krishnan and H. L. Friedman, *J. Phys. Chem.,* **75**, 3598 (1971).

Comparative Vibrational Spectroscopic Studies Between Nickel, Zinc Tetraphenylporphyrins and Tetraphenylchlorins

Ok-Keun Song and Min-Joong Yoon

Department of Chemistry, Chungnam National University, Chungnam 302-764

Jae-Rim Chang and Dongho Kim*

Optics Lab., Korea Standards Research Institute, Daedok Science Town, Chungnam 302-340

Received August 1, 1988

The infrared and resonance Raman spectra are reported for nickel and zinc tetraphenylchlorins. It is found that the IR and RR spectra become more complicated compared with the corresponding porphyrin analogs due to the symmetry changes. Some vibrational parameters like the core size and the symmetry change are examined in accordance with vibrational spectra of other type of chlorins.

Introduction

The vibrational spectroscopic studies on the metalloporphyrin through infrared (IR) and Raman spectroscopies have been actively carried out for the last 10 years.[1] The metalloporphyrins are model compounds which have been extensively studied *in vitro* to understand the nature of chemical bonds or the geometrical structure of macrocycle molecules and the electron transfer reaction or O_2 transfer mechanism in photosynthesis.[2] In metalloporphyrins the transition metal is inserted into the center of the extended aromatic ring; due to the long conjugation bond, there is a very strong absorption band in the visible range (Figure 1).[3] The d orbital of the central metal has a strong effect on the vibrational structure of the metalloporphyrin; consequently the spin state, the oxidation state and the size of the metal or the axial ligand effect have been examined relatively well through vibrational spectroscopic studies.

In metallochlorins the C_b-C_b bond of one of four pyrrole rings of the metalloporphyrin is saturated by hydrogens (Figure 1). Metallochlorins contribute to the biological catalytic function not only in chlorophylls but also in the prosthetic groups of various heme proteins, like metalloporphyrins.[4-8] Some resonance Raman (RR) and IR spectroscopic studies on chlorophylls,[9] bacterial cytochrome d,[10-12] leukocyte meyloperoxidase,[7,8] bovine spleen green heme protein[8] and sulfmyoglobin[6] have been reported. For the model compound, reports on RR spectra of M(II)OEC,[13-16] Ni(II)TMC[17] and Cu(II)TPC[17] were published by several groups and quite

M−TPP

X.Y Equivalence
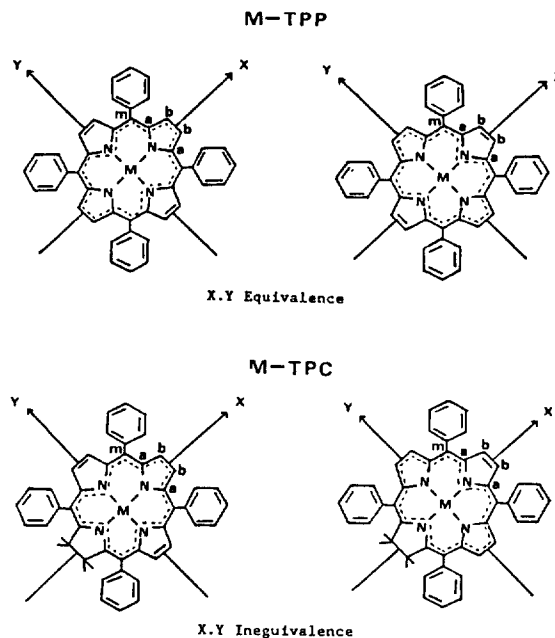
M−TPC

X.Y Inequivalence

Figure 1. Inner π electron conjugation pathways for a metalloporphyrin and a metallochlorin. a,b,m denote different carbon positions respectively and M respresents a metal.

recently the problem of assigning the chlorin vibrational spectrum was addressed by Bocian *et al.*[18] However, if the criteria of distinguishing between the porphyrin and the chlorin RR spectroscopic parameters are to be widely applicable to the verification of the presence of the chlorin

---

* To whom all correspondence should be addressed.

Effect of Parameters on the Retention of Benzenes in LC

Bull. Korean Chem. Soc., Vol. 10, No. 1, 1989 35

tor. Chromatograms were recorded on Bausch and Lomb Omniscribe Recorder. The detection wavelength was 254 nm and the sensitivity was set at 0.05 AUFS. The chart speed was 1.0 cm/min. and the flow rate of mobile phase was 1.0 ml/min.

Standard Solutions. Compounds were first grade or reagent grade chemicals and were purified by simple distillation or recrystalization. Standard solutions were prepared by dissolving the compounds in HPLC grade methanol and then by removing the particles greater than 0.5 μm with Waters Sample Clarification Kit.

Mobile Phases. For mobile phase, HPLC grade methanol and water were mixed by volume ratio. Each mixture was allowed to equilibrate for 1 hr. and then filtered through 0.5 μm Millipore organic filter. The gas bubbles in the solution were removed by vibrating the solution for about 20 min. in an ultrasonic bath.

Stationary Phases. Two columns were used: a 3.9 mm × 30 cm Waters μ-Bondapak C_{18} column and a 3.9 mm × 30 cm Waters μ-Bondapak phenyl column.

Measurements. The retention of solute is expressed by capacity factor, k'

$$k' = \frac{t_R - t_o}{t_o}$$

where t_R and t_o are the retention time of solute and methanol peak, respectively.

Results and Discussion

Two assumptions were made in this study. First, we assumed that solute-mobile phase interaction contributed more to the solute retention than solute-stationary phase interaction did. Therefore, we only considered the interaction between solute and mobile phase. Second, we assumed that the solvent molecule in the vicinity of the solute was different in behavior from that of the bulk solvent molecules.

So far, the parameter, which has been used to predict the solute retention thermodynamically or experimentally, describes bulk properties of solutes or mobile phases. But, it is not appropriate to explain the solute-mobile phase interaction with such bulk properties. Therefore, this study considered the parameter which represent the change in interaction between solute and the solvent molecules adjacent to the solute as the mobile phase changes. The correlations of dielectric increment-solute retention and mixed solvent solubility parameter-solute retention have been examined. The retention data of benzene and substituted benzene at different methanol compositions are shown in Table 1 and 2.

The Effect of Dielectric Increment on Solute Retention. When the polar solutes were added to the solution, the polarization phenomena were used to present the solute-solution interaction. Clausius and Mosotti[4] expressed the interaction between the external field and the polarization of the individual molecules. Onsagar[5] considered a molecule in solution as a cavity formed in the medium which has a homogeneous dielectric constant and determined the local field of the molecule.

When small amount of polar solute is added to the solution, the dielectric constant of the solution is given by the Onsagar equation as

where ε' is the dielectric increment, ε_1 and ε_2 are the dielec-

Table 1. Capacity Factor (k') of Monosubstituted Benzenes on μ-Bondapak C_{18} Column in CH_3OH-H_2O System

Substituted group	% CH_3OH								
	90	80	70	60	50	40	30	20	10
Benzene	0.68	0.98	1.86	2.38	5.00	10.15	14.52	20.77	33.70
CH_3	0.81	1.26	2.68	4.40	10.58	21.39	—	—	—
C_2H_5	0.91	1.41	3.78	7.10	17.60	—	—	—	—
F	0.63	0.93	1.93	2.81	5.71	12.42	—	—	—
Cl	0.80	1.26	2.78	4.54	10.00	26.77	—	—	—
Br	0.83	1.37	2.82	5.15	12.17	31.08	—	—	—
I	0.89	1.52	3.45	6.50	16.00	44.58	—	—	—
OH	0.46	0.53	0.78	0.98	1.68	3.05	4.10	6.36	10.78
NH_2	0.39	0.51	0.76	0.84	1.33	2.24	2.83	4.40	7.49
CH_2OH	0.47	0.52	0.83	0.98	1.68	3.03	4.43	7.13	13.04

Table 2. Capacity Factor (k') of Monosubstituted Benzenes on μ-Bondapak Phenyl Column in CH_3OH-H_2O System

Substituted group	% CH_3OH								
	90	80	70	60	50	40	30	20	10
Benzene	0.13	0.26	0.51	0.87	1.65	2.97	—	—	—
CH_3	0.16	0.33	0.68	1.28	2.75	5.21	—	—	—
C_2H_5	0.18	0.39	0.88	1.84	4.44	10.28	—	—	—
F	0.13	0.26	0.52	0.92	1.82	3.53	—	—	—
Cl	0.16	0.33	0.71	1.38	3.00	6.75	—	—	—
Br	0.18	0.39	0.79	1.57	3.60	8.50	—	—	—
I	0.20	0.43	0.92	1.93	4.85	11.13	—	—	—
OH	0.07	0.14	0.25	0.39	0.86	1.27	1.82	2.23	3.16
NH_2	0.12	0.16	0.29	0.43	0.93	1.46	1.68	2.89	4.22
CH_2OH	0.08	0.14	0.26	0.41	0.71	1.48	1.90	2.72	3.63

$$\varepsilon = \varepsilon_1 + [\frac{(\varepsilon_2 - 1)(2\varepsilon_2 + 1)}{2\varepsilon_2} - (\varepsilon_1 - 1)]\frac{v_2}{1000}C_2 \qquad (1)$$

$$\varepsilon' = [\frac{(\varepsilon_2 - 1)(2\varepsilon_2 + 1)}{2\varepsilon_2} - (\varepsilon_1 - 1)]\frac{v_2}{1000} \qquad (2)$$

tric constants of solvent and solute, respectively. v_2 is the solute molar volume and C_2 is the solute molarity. The dielectric increment, ε' describes the change in dielectric constant occurring between the solute and the surrounding solvent molecules in solution. It is a characteristic value of the solute in the system.[6]

The relationship between the solute retention and the dielectric increment, ε' was examined in Figure 1, 2 and 3. The plots have been obtained using the μ-Bondapak C_{18} column as the stationary phase and water-methanol mixtures as the mobile phase by varying composition of methanol from 10 to 90%.

The solutes examined in Figure 1 are phenol, aniline, and benzyl alcohol which form strong hydrogen bonding with methanol-water mixtures. The solute-solvent hydrogen bonding causes big increases in the dipole moment of solute by solvent effect which affects the electron migration.[7] From electrostatic considerations, the layer of solvent immediately surrounding the solute is made up predominantly of solvent
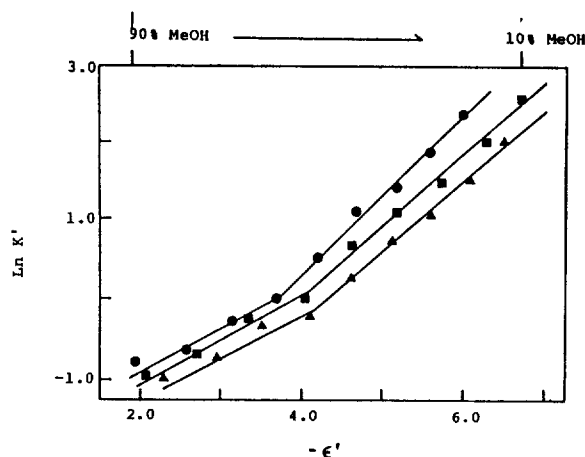
36 *Bull. Korean Chem. Soc., Vol. 10, No. 1, 1989*

Dai Woon Lee et al.

Figure 1. Relationship between dielectric increment$(-\varepsilon')$ and Ln k' values of phenol(●), aniline(▲), and benzyl alcohol(■) on the u-Bondapak C_{18} column.
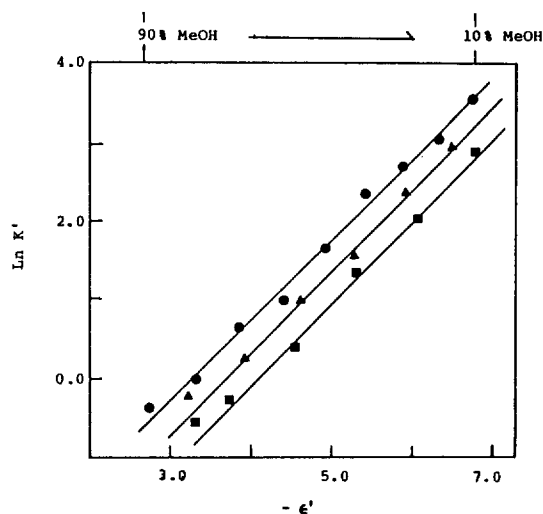

Figure 2. Relationship between dielectric increment $(-\varepsilon')$ and Ln k' values of benzene(●), toluene(▲), and ethylbenzene(■) on the u-Bondapak C_{18} column.

Figure 3. Relationship between dielectric increment $(-\varepsilon')$ and Ln k' values of fluorobenzene(●), chlorobenzene(▲), bromobenzene(○), and iodobenzene(△) on the u-Bondapak C_{18} column.

ment of solute will become reduced and a decrease in Keesom interaction will occur. As shown in Figure 1, the rate of increase in retention increases sharply compared to ε' above 60% methanol.

The dielectric increment, ε' is related to Keesom interaction[8] by

$$\varepsilon' = \frac{9}{2000} \left[20.6 \times 10^{36} \mu\bar{\mu} - \frac{(\varepsilon_0 - 1)(2\varepsilon_0 + 1)}{9\varepsilon_0} v + R\right] \quad (3)$$

where $\mu\bar{\mu}$ is the scalar product of the dipole moment, μ of the solute and dipole moment, $\bar{\mu}$ of the solute and its shell of neighbours, beyond which the dielectric constant equals the macroscopically observed dielectric constant. ε_0 is the dielectric constant of the solvent, v is the molar volume of the solute and R is its molar refractivity. Therefore, a decrease in dielectric increment also decreases Keesom interaction. In general, the decrease in methanol composition increases dielectric constant of mobile phase and thus decreases dielectric increment by eqn.(3). The solvent shell of increased dielectric constant causes an increase in electrostatic shielding effect and thus results in a decrease in the effective dipole moment of solute. As a result, Keesom interaction is reduced and thus solute retention is increased.

Figure 2 and 3 are the plots of alkylbenzenes and halobenzenes, respectively. Since these solutes do not form hydrogen bondings, only the dielectric constant contributes to the solute retention and thus the natural logarithm of retention factor (ln k') is linearly dependent on ε'. In the case of halobenzenes, the points are closely located around the line. This is due to their similar dipole moments.

Figure 4, 5 and 6 show the interactions between the solute and mobile phase, water-methanol mixture, on the μ-Bondapak phenyl column. Different trend from Figure 1 was observed in Figure 4. This may be the result of interaction between the solute and phenyl group of the stationary phase which has been ignored in case of the C_{18} column. However, Figure 5 and 6 show similar tendency to Figure 2 and 3 since alkylbenzenes and halobenzenes do not form hydrogen bondings. Thus, the observed retention behavior can be seen

mixture constituent having the higher dielectric constant. Therefore, the shell of solvent constituent of higher dielectric constant serves to act as an electrostatic shield and thus decreases the effective dipole moment of the solute.[8]

When the solutes in Figure 1 form hydrogen bonding with methanol-water mixture, the solutes act as a proton-donor and methanol acts as a proton-acceptor. Thus, an increase in methanol composition in mobile phase leads to stronger hydrogen bondings and a larger dipole moment. Since the dielectric constant of mobile phase becomes smaller as the methanol composition increases, the effect of dielectric constant on the dipole moment will decrease compared to the effect of hydrogen bonding on the dipole moment. Therefore, the effective dipole moment of solute increases. As a result, increased Keesom interaction between the solute and mobile phase decreases solute retention.

However, at compositions less than 60% methanol, the dielectric constant of mobile phase becomes bigger and the hydrogen bonding between solute and mobile phase becomes weaker. As a consequence of shielding effect of bigger dielectric constant of mobile phase, the effective dipole mo-
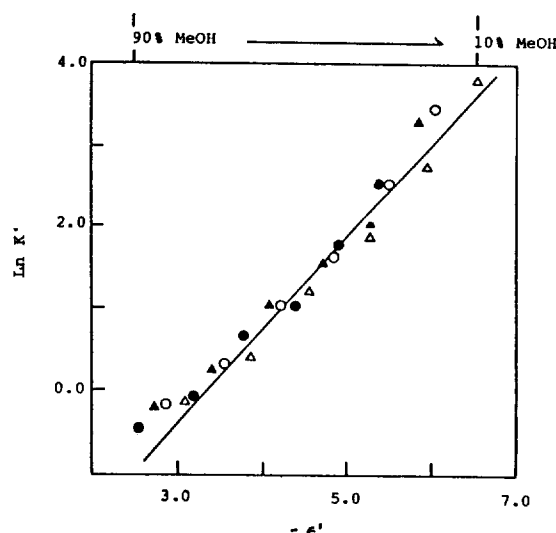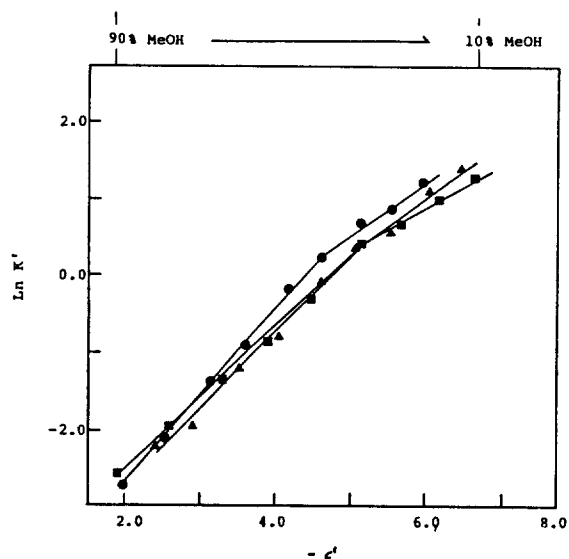
Figure 4. Relationship between dielectric increment $(-\varepsilon')$ and Ln k' values of phenol(●), aniline(▲), and benzyl alcohol(■) on the u-Bondapak phenyl column.
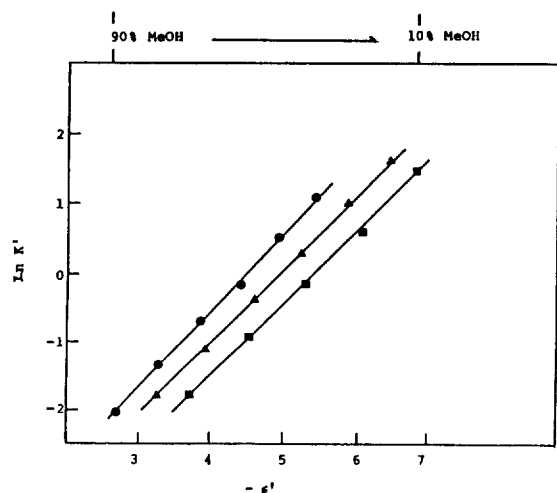

Figure 5. Relationship between dielectric increment $(-\varepsilon')$ and Ln k' values of benzene(●), toluene(▲), and ethyl benzene(■) on the μ-Bondapak phenyl column.

Figure 6. Relationship between dielectric increment $(-\varepsilon')$ and Ln k' values of fluorobenzene(●), chlorobenzene(▲), bromobenzene(○), and iodobenzene(△) on the μ-Bondapak phenyl column.

Table 3. Physical Properties of Monosubstituted Benzenes[a]

Sample	MW	MV	ϵ	μ
Benzene	78.11	88.86	2.28	0.00
Toluene	92.13	106.40	2.38	0.36
Ethylbenzene	106.16	122.46	2.40	0.59
Fluorobenzene	96.10	93.86	5.42	1.60
Chlorobenzene	112.56	101.77	5.62	1.69
Bromobenzene	157.02	105.03	5.40	1.70
Iodobenzene	204.02	111.85	4.63	1.70
Phenol	94.11	87.87	9.78	1.45
Aniline	93.13	91.13	6.89	1.53
Benzyl alcohol	108.13	103.60	13.60	1.71

MW: Molecular weight MV : Molar volume (cm³/mole) ϵ : Dielectric constant (C²/J·m) μ : Dipole moment (D) [a]Reference 9.

that phenyl column shows different behavior for the high-polarity solutes such as phenol, aniline, and benzyl alcohol whereas it shows similar behavior for the low-polarity solutes compared with C_{18} column.

As examined above, the use of dielectric increment, which represent the interaction between the solute and the solvent adjacent to the solute, will be helpful to get a quantitative relationship on the solute retention.

Effect of Solubility Parameter on Solute Retention. The correlation between the solute retention and solubility parameter has been examined because the solute-mobile phase interaction is related to solubility. In condensed phases (solids, liquids, solutions) strong attractive forces exist between molecules, and as a result each molecule has a considerable (negative) potential energy. This potential energy is called the cohesive energy, $- E$. The correlation between the cohesive energy per unit volume (cohesive energy density) and solubility parameter δ is[9]
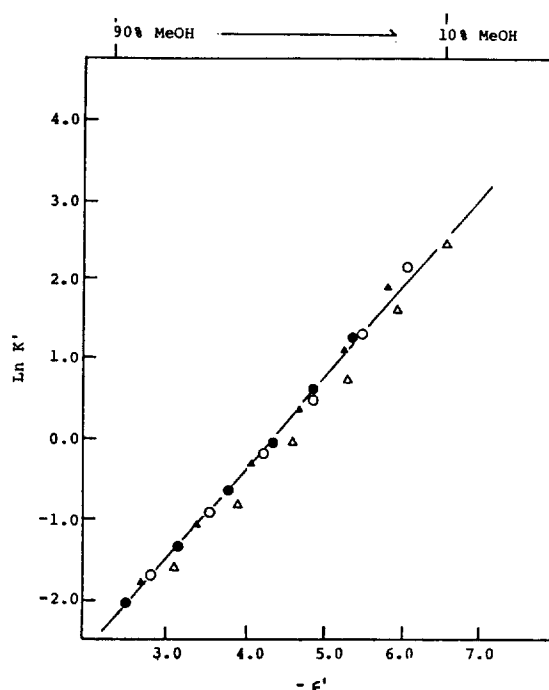
$$\delta = (-\frac{E}{V})^{1/2} \tag{4}$$

There are three modes of interaction between molecules which collectively produce the cohesive energy characteristic of the liquid state: (i) dispersion or London force; (ii) polar interactions; (iii) specific chemical interactions, notably hydrogen bonding.

$$-E = -E_d - E_p - E_h \tag{5}$$

$$-\frac{E}{V} = -\frac{E_d}{V} - \frac{E_p}{V} - \frac{E_h}{V}$$

$$\text{or}\quad \delta_o^2 = \delta_d^2 + \delta_p^2 + \delta_h^2 \tag{6}$$

The solubility parameter values of solutes and solvents used in this study are shown in Table 3. In general, δ_o values de-
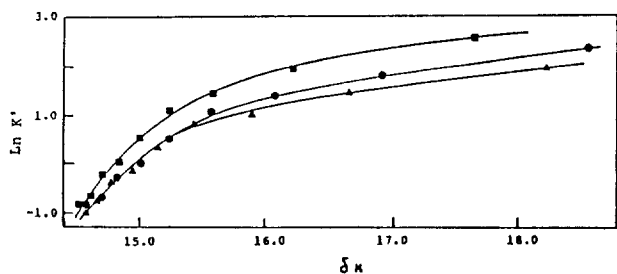
38 *Bull. Korean Chem. Soc., Vol. 10, No. 1, 1989*

Dai Woon Lee et al.

Figure 7. Plots of ln k' vs. δ_M of phenol($\bullet$), aniline($\blacktriangle$), and benzyl alcohol($\blacksquare$). The chromatographic conditions are the same as in Figure 1.
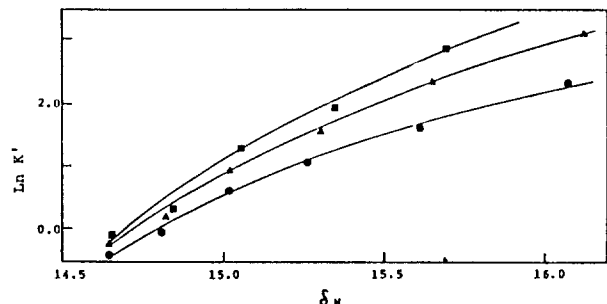
Figure 8. Plots of ln k' vs. δ_M of benzene($\bullet$), toluene($\blacktriangle$), and ethyl-benzene($\blacksquare$). The chromatographic conditions are the same as in Figure 1.

crease regularly with increasing E_d, indicating the dominating contribution to δ_o of polar and hydrogen bonding forces in most liquids.

The solubility parameter of a solute in the binary solvent mixture, δ_M is defined by using an "effective volume fraction", Φ^* term.[10] This term reflects the nearest neighbour solvent environment of a solute with the preferential solvation by one of the solvent components.

$$\delta_M = \Phi_1^* \delta_1 + \Phi_3^* \delta_3$$

$$\frac{\Phi_1^*}{\Phi_3^*} = \frac{\Phi_1 (\delta_2 - \delta_3)^2}{\Phi_3 (\delta_2 - \delta_1)^2}, \quad \Phi_1^* + \Phi_3^* = 1 \tag{7}$$

where δ is the solubility parameter, Φ is volume fraction, subscripts M, 1, 2, and 3 denote mixed solvent, water, solute, and methanol, respectively. Volume fraction, Φ is defined as[11]

$$\Phi_1 \equiv \frac{n_1}{n_1 + mn_3}, \quad \Phi_3 \equiv \frac{mn_3}{n_1 + mn_3} \tag{8}$$

where n is the mole of solvent and m is the molar volume ratio of water and methanol.

Figure 7, 8 and 9 are the plots of solute retention as a function of solubility parameter of mixed solvent, δ_M in water-methanol mixtures by varying composition on the μ-Bondapak C_{18} column. As the composition of mobile phase changes progressively from pure water to pure methanol, cohesive energy changes. The change in cohesive energy affects the energy state between the solute and mobile phase. This results in a change in solubility of solute in mixed mobile phase as expressed by eq. 7.

Krishnan et al.[12] showed the following approximate equation for the desolvation enthalpy of solute Y in solvent S

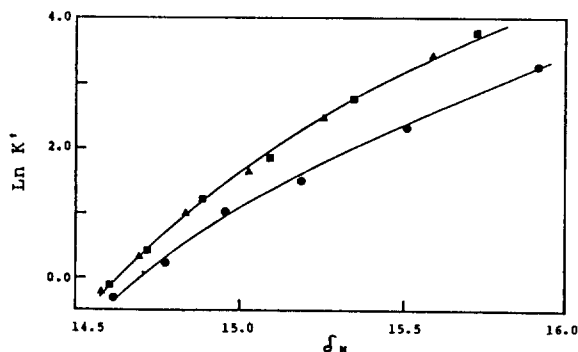$$(Y)_{g \leftarrow s} = (Y)_{g \leftarrow s}^{el} + (Y)_{g \leftarrow s}^{sp} \tag{9}$$

Figure 9. Plots of ln k' vs. δ_M of chlorobenzene($\bullet$), bromobenzene($\blacktriangle$), and iodobenzene($\blacksquare$). The chromatographic conditions are the same as in Figure 1.

Here the electrical contribution derives from the interaction of the electrical dipole of a solvent molecule with the polarizability of the solute. The solubility parameter contribution to eq. (9) is

$$(Y)_{g \leftarrow s}^{sp} \equiv V_Y \delta_s (2 \delta_Y - \delta_s) \tag{10}$$

where V_Y is the molar volume of the solute and the $\delta_x's$ are the solubility parameters of species X. The solubility parameter contribution is again regarded as two terms. The term $-V_Y \delta_s^2$ accounts for the enthalpy associated with the formation of a cavity in the solvent to accommodate the solute particle. The term $2\delta_Y \delta_S \delta_Y$ accounts for the enthalpy of interaction by van der Waals forces of the solute with the solvent molecules next to it in solution.

The linearity of solvation energy cannot be expected as to methanol composition changes in water-methanol mixture. Since the change in solubility parameter with change in cohesive energy is related to the solvation energy of solute, nonlinearity between the solute retention and solubility parameter in mixed solvent, δ_M is observed such as the relationship between solute retention and surface tension of mobile phase.[2] As examined above, the parameters representing the bulk properties of solute, such as solubility parameter, dielectric constant, and polarity are not appropriate to represent the solubility of solute in the system containing the polar non-electrolyte in the reactive solvent. But parameters representing the interaction between solute and the solvent adjacent to the solute are capable of explaining the solute solubility. By using the parameters, dielectric increment ϵ' and mixed solvent solubility parameter δ_M which represent the change occurring between the solute and its adjacent solvent, it is expected to get better results in predicting the retention.

References

1. C. Horvath and W. Melander, *J. Chromatogr. Sci.*,**15**, 393 (1977).
2. C. Horvath and W. Melander, *J. Chromatogr.*, **125**, 129 (1976).
3. P. Jandera, H. Colin, and G. Guiochon, *Anal. Chem.*, **54**, 435 (1982).
4. J. H. Hildebrand and R. L. Scott, "The Solubility of Nonelectrolytes", 3rd ed., Chap. IX, Reinhold Pub-
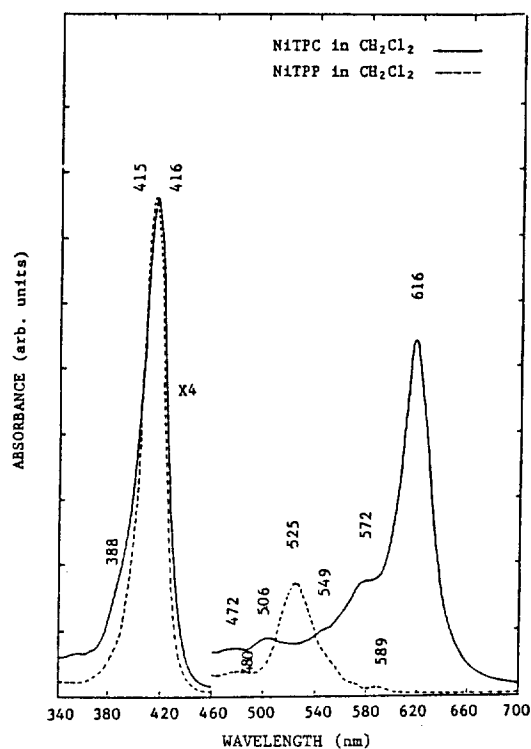
40 *Bull. Korean Chem. Soc., Vol. 10, No. 1, 1989*

Ok-Keun Song et al.

Figure 2. Absorption spectra of NiTPC (solid line) and NiTPP (dashed line) in dichloromethane.

Figure 3. Absorption spectra of ZnTPC (solid line) and ZnTPP (dashed line) in dichloromethane.

molecule in a biological system of undefined prosthetic groups, it is necessary to demonstrate that such parameters can be extended to the meso substituted metallochlorins like M(II)TPC. In this article, some characterization studies on the vibrational parameters of the structure such as the symmetry and the core size dependences have been performed through the comparision the IR and RR results of Ni(II)TPP and Zn(II)TPP with those of Ni(II)TPC and Zn(II)TPC.

Experimental

NiTPP and ZnTPP were purchased from Aldrich. NiTPC and ZnTPC were synthethized through the metal insertion into the TPC which was made through the diimide reduction of TPP.[19] The metal insertion was accomplished by heating a CHCl₃ solution of the TPC with metal acetate which was dissolved in methanol.[20] The metallochlorins were purified by elution on Fisher A-540 alumina when necessary and the purities were checked by absorption spectrum using a Cary 219 UV-Vis. spectrophotometer.

The IR spectra were obtained from KBr pellets on a DIGILAB Model FTS 80 FTIR instrument. For the Raman measurements, the KBr pellet with a little K_2SO_4 as an internal standard was attached to the copper cold finger of the liquid nitrogen Raman cell. The liquid nitrogen temperature provides advantages over the solution Raman spectrum acquired at room temperature mainly in obtaining a high-resolution Raman spectrum and avoiding any possible sample degradation caused by a local heating with a tightly-focused laser beam. The details of Raman spectrum collection system were given elsewhere.[21] Briefly, a Spectra Physics 165 Ar ion laser was used to illuminate the sample by quasi-back-scattering geometry. The scattered light was collected by an $f = 1.2$ camera lens and focused onto the 1 meter Jobin-
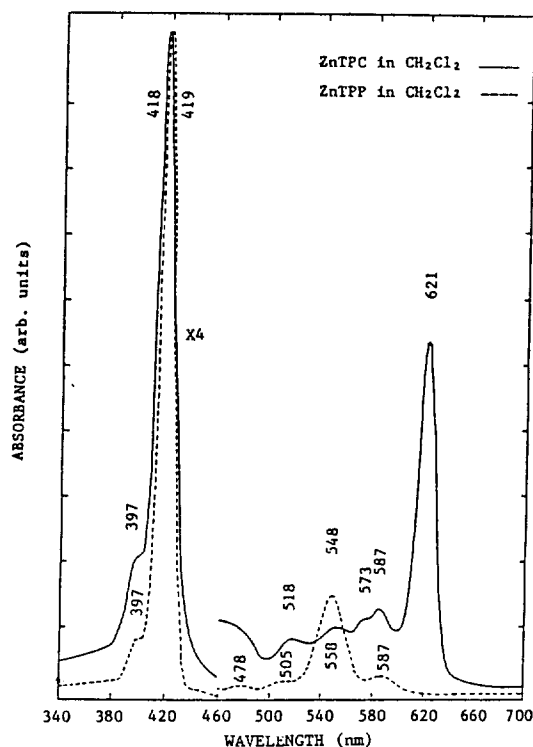
Yvon Raman U-1000 double monochrometer using an $f = 30$ cm planar convex lens. A Hamamatsu R943-02 photomultiplier tube, cooled to -20 C with a Hamamatsu C2761 PMT cooler, was used as a detector. After the amplification of the output current of the PMT, the Hamamatsu C1230 photon counter and discriminator were used for photon counting detection. The analog signal from the photon counter was converted to the digital signal by A/D converter. The NEC PC9801V computer controls the scanning of the monochrometer and the data was stored in the computer and plotted by Roland 980A XY digital plotter.

Results and Discussions

A. Metallochlorin Molecular Symmetry and Electronic Structure

As shown in Figure 1, the metallochlorin has the structure where one of four pyrrole rings in the metalloporphyrin is saturated by hydrogens. From the previous X-ray crystallographic study, the metalloporphyrin has a flat structure and belongs to the D_{4h} symmetry group with the center of inversion.[22] However for the metallochlorin, an extremely nonplanar geometry, with S_4 ruffled structure, without the center of inversion was found from previous studies.[23-25]

The macrocycle π electron conjugation pathway of the metalloporphyrin is equivalent in both x and y directions. However, that of the metallochlorin is not.[3] Thus, this x,y inequivalence reveals that the degeneracy in the two pairs of orbitals composed of four-orbital model is broken.[3,15] Among the possible four transitions, two are strongly allowed transitions, which make the split Soret (or B) bands or one Soret band if an accidental degeneracy occurs. The lowest energy Q transition is more strongly allowed relative to that of porphyrins. Thus the characteristic intense 600 nm peak for the

Comparative Vibrational Spectroscopic Studies

Bull. Korean Chem. Soc., Vol. 10, No. 1, 1989 41

Table 1. Peak Position and Origins of UV-Vis. Absorption Spectra of NiTPC AND ZnTPC

Origin Sample	$Q_y(0,0)$	$Q_y(0,1)$	$Q_y(0,2)$	$Q_x(0,0)$	$Q_x(0,1)$	B_y	B_x
NiTPC	616	572	549	506	472	416	388
ZnTPC	621	587	573	558	518	418	397

Table 2. Symmetry Groups and Raman Allowed Modes

D_{4h}	$C_2(x)$
$A_{1g}(p)$	A(p)
$B_{2g}(dp)$	A(p)
$A_{2g}(ap)$	B(dp or ap)
$B_{2g}(dp)$	B(dp or ap)
E_u(forbidden)	A + B(p + dp or ap)

chlorin is usually observed; the other Q transitions are almost parity forbidden and consequently weak.[3] Therefore from the UV-Vis absorption spectra (Figures 2 and 3), the NiTPC spectra has stronger and lower energy Q band compared with the NiTPP spectra and there is a high energy shoulder on the Soret band. For ZnTPC (Figure 3), similar behavior is observed, however the Soret and Q bands show more sharp structure compared with those of NiTPC. Equivalent behavior was observed in the cases of NiTMC and NiTPP. Thus the relative broadening of the UV-Vis absorption spectra for nickel porphyrin and chlorin is a characteristic of the nickel metal. The peak positions and the origins of the UV-Vis. absorption spectra are tabulated in Table 1.

B. IR and RR properties

Since the metalloporphyrin has an inversion center, the IR and Raman allowed vibrational modes are mutually exclusive. Thus for the metalloporphyrin with D_{4h} symmetry, in-plane E_u and out-of-plane A_{2u} modes are IR active and $A_{1g}(p)$, $B_{1g}(dp)$, $A_{2g}(ap)$ and $B_{2g}(dp)$ modes (p: polarized, dp: depolarized, ap: anomalously polarized) are Raman active. Almost no correlation can be found between IR and Raman frequencies of the MTPP.[1] However, the symmetry lowering from the D_{4h} symmetry of MTPP to the $C_2(x)$ symmetry of MTPC causes the Raman inactive modes to be allowed ones and the degenerate E_u modes split into A and B modes.[1] Generally the followings are expected for the RR behavior due to the symmetry change from the metalloporphyrin to the metallochlorin (Table 2).

(a) all $B_{1g}(dp)$ porphyrin vibrational modes should become A(p) vibrational modes.

(b) $A_{2g}(ap)$ and $B_{2g}(dp)$ porphyrin modes should become B (dp or ap) modes.

(c) E_u (doubly degenerate) porphyrin modes should be split into A and B components.

The alteration in molecular symmetry also results in an increase in the total number of vibrational bands observed as well as an increase in the number of totally symmetric polarized Raman bands relative to the RR spectrum of an analogous porphyrin complex.[1] For the porphyrin, the excitation in the neighborhood of the strongly allowed Soret absorption band produces strong enhancement of Franck-Condon-active A_{1g} modes, while in the neighborhood of the quasi-forbidden Q bands produces selective enhancement of vibronically active A_{2g}, B_{1g} and B_{2g} modes.[1] In addition, normally A_{2g} modes
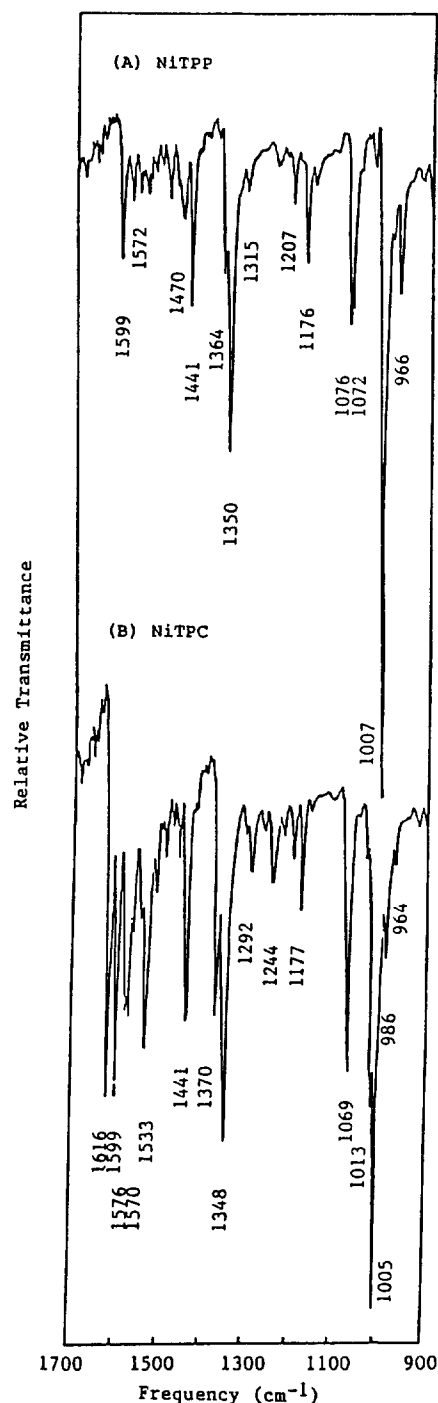
Figure 4. Infrared spectra of NiTPP(top) and NiTPC(bottom) in KBr pellet at room temperature.

are seen only with Q-band excitation, enhancement being provided by their role in Q-B vibronic mixing and B_{1g} modes can frequently be seen with Soret excitation, because of their role in Jahn-Teller splitting of the doubly degenerate excited states. In contrast, for chlorin the resonance enhancement pattern of RR frequencies is distinctly different from that of porphyrin. The polarized bands dominate the NiOEC RR spectra obtained with B and Q excitations, as has been observed for other metallochlorins, while ap and dp modes dominate the spectrum obtained with Q_x excitation. Also it was found that ap and dp modes are clearly observed with B band
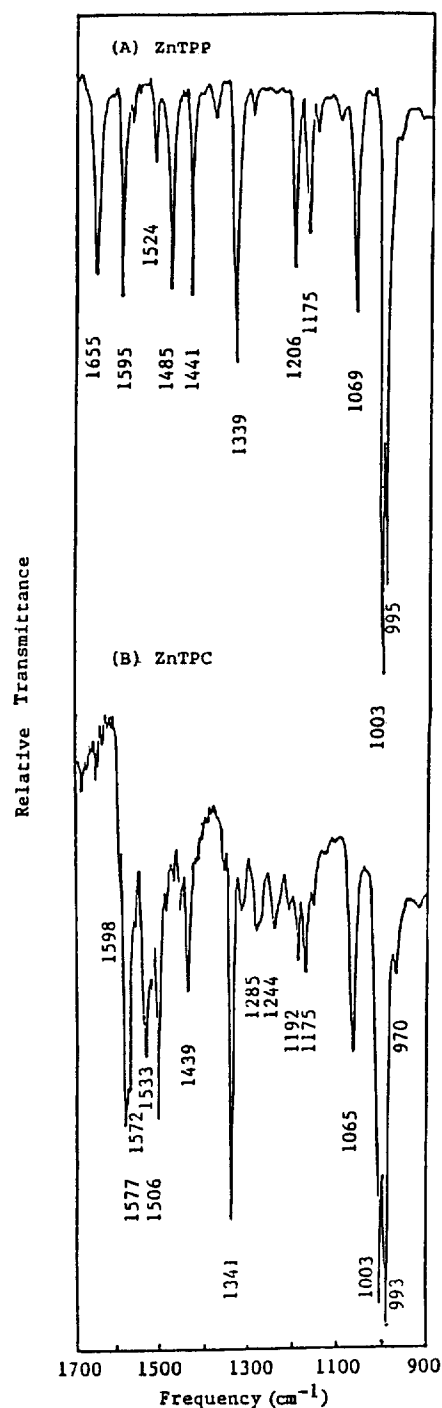
42 *Bull. Korean Chem. Soc., Vol. 10, No. 1, 1989*

Ok-Keun Song et al.

Figure 5. Infrared spectra of ZnTPP(top) and ZnTPC(bottom) in KBr pellet at room temperature.

trivial problem to assign the modes properly. Even though there have been accumulated RR spectroscopic studies on MTPP analogs, the vibrational modes were recently catalogued and revised.[26] In the cases of MTPP's, the different substituent patterns relative to MOEP lead to appreciable differences in the vibrational patterns. However a rough correspondence among the skeletal modes is found, except that the mode numbering shifts by one in the B_{1g} and A_{2g} blocks, due to the missing of C-H stretching mode in TPP compared to other porphyrins. Recent study revised the mode assignment at ~1450 cm^{-1} region and as a $\nu_{28}(B_{2g})$ C_a-C_b pyrrole bond stretching mode based on the core size correlation which was previously assigned as a $\nu_{13}(B_{1g})$ C_a-N mode.[26]

Thus, combined with the RR spectra obtained with various excitations, polarization measurements and comparision with MTPP vibrational frequencies, the efforts are made to assign the vibrational modes of MTPC which have not been studied systematically.

IR properties of NiTPC and ZnTPC. High-frequency IR spectra of NiTPP, NiTPC, ZnTPP and ZnTPC are presented in Figures 4 and 5; the IR frequencies and mode assignments are tabulated in Tables 3 and 4. For NiTPP and ZnTPP, IR frequencies at 1599, 1350, 1007 cm^{-1} (NiTPP) and 1595, 1339, 1003 cm^{-1} (ZnTPP) (A, B, F-phenyl modes, respectively) are known to be due to the meso-substituted phenyl mode contributions.[17] And ν_{38}, ν_{39}, ν_{40}, ν_{41} and ν_{44} modes can be assigned as IR active C_b-C_b, C_a-C_m, C_b-C_b, C_a-N stretching modes and asymmetric bending of C_bH modes, respectively (Tables 3 and 4).[18] Here, ν_{42} and ν_{43} modes are missing, because these modes are assigned previously as ethyl mode contributions of MOEP analogs. Generally, for NiTPP and ZnTPP IR and RR bands are mutually exclusive as expected for D_{4h} symmetry. On the contrary, for NiTPC and ZnTPC the IR and Raman active vibrational modes are no longer exclusive and each vibrational spectrum becomes more complicated due to the symmetry lowering compared to the TPP analogs. Thus there are many new bands in IR spectrum which are also present in RR spectrum. Additionally, as expected, the splitting of E_u modes occurs especially for the ν_{38}, ν_{39}, ν_{41}, ν_{44} modes for ZnTPC and ν_{38}, ν_{39}, ν_{40} modes for NiTPC. These split modes are no longer Raman forbidden, because E_u modes are split into A and B modes which are also Raman active. The phenyl modes (A, B, F-phenyl for NiTPC and A, F-phenyl for ZnTPC) are preserved relative to the MTPP. And the altered intensity pattern around 1600 cm^{-1} is evident. For NiTPC 1599 cm^{-1} band is due to the phenyl mode contribution and 1616 cm^{-1} band is either a characteristic chlorin band as assigned by Andersson et al.[17] or $\nu_{37}(A)$ $C_a C_m$ stretching mode which are normally observed for other metalloporphyrins. For ZnTPC the band at 1598 cm^{-1} is attributable to the phenyl mode contribution and for 1655 cm^{-1} band the same analogy might be applicable to the NiTPC case. The ν_{44} modes of ZnTPP and NiTPP are assigned as a pyrrole-hydrogen bending mode by Andersson et al.[17] This band seems to be existent in NiTPC and ZnTPC without a major change in frequencies and intensity pattern. The altered band pattern in the 900-1000 cm^{-1} region for NiTPC and ZnTPC is particularly noticeable, and is not fully understood, especially for 993 cm^{-1} band for ZnTPC and 1013 cm^{-1} band for NiTPC, which are not present in the RR spectra. However we can not preclude the possibility of mixing in IR and RR bands for MTPC cases due to the sym-

excitation.[18] Thus, from these observations it is necessary to obtain RR spectra with B, Q_x and Q_y excitations in order to observe all of the skeletal modes. Not only the different resonance enhancement pattern of RR modes, but also the polarization ratio of RR modes is quite helpful in determining the origins of each mode, which has not been accomplished yet for MTPC's. However the actual polarization ratio deviates from the ideal values because the symmetry of the metallochlorin is lower than D_{4h}, but the qualitative application is still effective in the mode assignment of the metallochlorin.[18] Considering these characteristics, it is not a

Comparative Vibrational Spectroscopic Studies

Bull. Korean Chem. Soc., Vol. 10, No. 1, 1989 43

Table 3. R R and IR Frequencies of NiTPP and NiTPC[**]

RR						IR					
NiTPP			NiTPC			NiTPP			NiTPC		
1596^{vs}	A-phenyl		1616^{s}	$\nu_{37}C_aC_m$	A				1616^{s}	$\nu_{37}C_aC_m$	
			1599^{m}	A-phenyl		1599^{m}	A-phenyl		1599^{s}	A-phenyl	
			1579^{s}	$\nu_{38}C_bC_b$(ap)	B				1576^{s}	$\nu_{38}C_bC_b$	(1)
1574^{m}	$\nu_2C_bC_b$(p)	A_{1g}	1572^{s}	$\nu_2C_bC_b$(p)	A	1572^{w}	$\nu_{38}C_bC_b$	E_u			
									1570^{s}	$\nu_{38}C_bC_b$	(2)
									1560^{m}	$\nu_{39}C_aC_m$	(1)
1553^{vs}	$\nu_{20}C_aC_m$(ap)	A_{2g}	1549^{m}	$\nu_{20}C_aC_m$(ap	B	1550^{w}	$\nu_{39}C_aC_m$	E_u			
									1541^{m}	$\nu_{39}C_aC_m$	(2)
			1535^{m}	$\nu_{40}C_bC_b$(p)	A				1533^{s}	$\nu_{40}C_bC_b$	(1)
			1512^{s}	$\nu_{40}C_bC_b$(dp)	B				1508^{w}	$\nu_{40}C_bC_b$	(2)
1503^{s}	$\nu_{12}C_bC_b$(dp)	B_{1g}							1489^{w}	$\nu_{12}C_bC_b$	
1486^{w}	$\nu_{28}C_aC_b$(dp)	B_{2g}				1470^{w}			1470^{w}		
1457^{w}	$\nu_3C_bC_b$(p)	A_{1g}							1458^{w}	$\nu_3C_bC_b$	
1437^{w}						1441^{m}			1441^{s}		
1377^{vs}	ν_4C_aN(p)	A_{1g}	1380^{s}	ν_4C_aN(p)	A						
			1370^{s}	$\nu_{41}C_aN$(dp)	B				1370^{s}	$\nu_{41}C_aN$	(1)
			1364^{s}	$\nu_{41}C_aN$(p)	A	1364^{m}	$\nu_{41}C_aN$	E_u			
1355^{w}	$\nu_{13}C_aN$(dp)	B_{1g}	1355^{s}	$\nu_{13}C_aN$(dp)	B						
			1349^{s}	B-phenyl		1350^{s}	B-phenyl		1348^{s}	B-phenyl	
									1292^{m}		
1242^{m}	$\nu_{22}\delta_{as}C_m$-ph(ap)		1242^{m}	$\nu_{22}\delta_{as}C_m$-ph(ap)	B				1244^{m}	$\nu_{22}\delta_{as}C_m$-ph	
1233^{m}	C-phenyl										
			1219^{m}								
1190^{m}	$\nu_{14}C_aC_b$(dp)	B_{1g}	1195^{m}	$\nu_{14}C_aC_b$(dp)	B				1196^{w}	$\nu_{14}C_aC_b$	
						1177^{m}					
1077^{m}	$\nu_{15}\delta_sC_bH$(dp)	B_{1g}	1075^{m}	$\nu_{44}\delta_{as}C_bH$(p)	A	1076^{m}					
1072^{m}	$\nu_5\delta C_bH$(p)	A_{1g}				1072^{s}	$\nu_{44}\delta_{as}C_bH$	E_u	1069^{s}	$\nu_{44}\delta_{as}C_bH$	(2)
1033^{w}	E-phenyl										
									1013^{s}		
1004^{vs}	f-phenyl		1005^{s}	F-phenyl		1007^{vs}	F-phenyl		1005^{vs}	F-phenyl	
992^{w}			997^{w}			978^{m}			986^{m}		
963^{m}						966^{m}			964^{m}		

[**]vs(very strong), s(strong), m(medium), and w(weak) represent the peak intensities. A_{1g}, A_{2g}, B_{1g}, B_{2g}, A and B denote the symmetry groups of each mode, (1) and (2) represent the splitting mode into high- and low-frequencies from IR active E_u modes. p(polarized), dp(depolarized) and ap(anomalously polarized) denote the polarization ratio of each mode, as and s mean asymmetric and symmetric motion repectively.

metry change. For example, for ν_{37}-ν_{44} bands of ZnTPC and NiTPC, these bands might be mixed with ν_{10}, ν_{11}, ν_{20}, ν_2 and ν_4 bands. However in our studies, the mode assignment for MTPC is made through the comparision with the corresponding MTPP frequencies under the assumption that the frequencies are not so different from each other, even though the enhancement pattern is different.

Resonance Raman Properties of NiTPC and ZnTPC. Resonance Raman spectra of NiTPP, NiTPC, ZnTPP and ZnTPC are shown in Figures 6, 7, 8 and 9 with various excitation conditions; their frequencies and mode assignments are tabulated in Tables 3 and 4. The NiTPP and ZnTPP spectra are generally in good agreement with previous works[1] except for 2-5 cm^{-1} frequency differences for some modes, which is probably caused by the sample condition (in our study the solid sample at 77 K was used for RR measurements). Nevertheless for NiTPP, the RR spectra are relatively simple; the two polarized bands at 1574 and 1377 cm^{-1} are assignable to the porphyrin skeletal modes ν_2 and ν_4

respectively, while the polarized bands at 1596, 1233, 1033 and 1004 cm^{-1} are due to the A, C, E and F-phenyl mode contributions on the basis of the previous work on (FeTPP)$_2$O.[27] The bands at 1553 and 1242 cm^{-1} show anomalously polarized character by the polarization measurements. However the band around 1553 cm^{-1} is still moderately enhanced via 457.9 nm excitation. This behavior is probably ascribable to the mixing of ν_{20}(ap) and ν_{11}(dp) modes at the same frequency because, for D_{4h} symmetry, the ap modes are not enhanced by the excitation in the neighborhood of Soret band. The other RR bands and corresponding mode assignments are tabulated in Table 3.

For NiTPC, the RR spectra are more complicated to NiTPP, as expected. The 1616 cm^{-1} mode can be assigned as characteristic chlorin mode or ν_{37}. The 1599, 1349 and 1005 cm^{-1} bands are believed to be the A, B and F-phenyl mode contributions by comparision with IR frequencies of NiTPC and vibrational mode assignments of NiTPP. The 1579 and 1572 cm^{-1} bands have different polarization behaviors, thus

Ok-Keun Song et al.

Table 4. RR and IR Frequencies of ZnTPP and ZnTPC

RR						IR					
ZnTPP			ZnTPC			ZnTPP			ZnTPC		
						1655^s	$\nu_{37}C_aC_m$	E$_u$			
1595^m	A-phenyl		1597^w	A-phenyl		1595^s	A-phenyl		1598^w	A-phenyl	
			1579^s	$\nu_{38}C_bC_b$(p)	A				1578	$\nu_{38}C_bC_b$	(1)
						1576^{vs}	$\nu_{38}C_bC_b$	E$_u$			
			1571	$\nu_{38}C_bC_b$(dp)	B				1572^s	$\nu_{38}C_bC_b$	(2)
1556^m	$\nu_{20}C_aC_m$(ap) A$_{2g}$										
1547^s	$\nu_2C_bC_b$(p) A$_{1g}$		1546^m	$\nu_2C_bC_b$(p)	A				1540^m	$\nu_2C_bC_b$	
			1537^s	$\nu_{39}C_aC_m$(ap)	B				1533^s	$\nu_{39}C_aC_m$	(1)
			1521^m	$\nu_{40}C_bC_b$(p)	A	1524^m	$\nu_{39}C_aC_m$	E$_u$			
			1507^s	$\nu_{39}C_aC_m$(p)	A				1506^s	$\nu_{39}C_aC_m$	(2)
1490^m	$\nu_{12}C_bC_b$(dp) B$_{1g}$					1485^s	$\nu_{40}C_bC_b$	E$_u$			
									1458^w	$\nu_3C_bC_b$	
						1441^s			1439^s		
			1365^m	$\nu_{41}C_aN$(p)	A				1364^w	$\nu_{41}C_aN$	(1)
1355^s	$\nu_{13}C_aN$(dp) B$_{1g}$		1359^s	$\nu_{13}C_aN$(dp)	B	1350^s	$\nu_{41}C_aN$	E$_u$			
1353^{vs}	ν_4C_aN(p) A$_{1g}$		1354^s	ν_4C_aN(p)	A						
			1340^s	$\nu_{41}C_aN$(dp)	B				1341^{vs}	$\nu_{41}C_aN$	(2)
						1339^s	B-phenyl				
			1295^s	(p)					1285^m		
			1245^s	(dp)					1244^m		
1236^s	C-phenyl		1239^m	C-phenyl							
						1206^s					
			1191^m	$\nu_{14}C_aC_b$(dp)	B				1192^m	$\nu_{14}C_aC_b$	
1173^m	$\nu_{14}C_aC_b$(dp) B$_{1g}$					1175^s			1175^m		
			1073^m	$\nu_{44}\nu_{as}C_bH$	A						
						1069^s	$\nu_{44}\delta_{as}C_bH$	E$_u$			
1070^m	ν_5 C$_b$H(p) A$_{1g}$		1065^w	$\nu_{44}\delta_{as}C_bH$(dp)	B				1065^s	$\nu_{44}\delta_{as}C_bH$	(2)
			1034^w	E-phenyl							
1004^m	F-phenyl		1004^s	F-phenyl		1003^{vs}	F-phenyl		1003^{vs}	F-phenyl	
995^w			996^w			995^{vs}			993^{vs}		

the former one is due to the ν_{38}(B) mode contribution which is no longer Raman forbidden and the latter one to the ν_2 mode. However in this mode the contribution of ν_{38}(A) mode caused by the splitting of ν_{38}(E$_u$) into ν_{38}(A) and ν_{38}(B) is possible.[18] The 1549 cm^{-1} band is probably due to ν_{20} because of the ap character; 1535 and 1512 cm bands are assigned as ν_{40}(A) and ν_{40}(B). The interesting feature of MTPC relative to MTPP, there are many strong bands around 1300–1400 cm^{-1}, where normally only one strong band ν_4(A$_{1g}$) is observed for TPP. To assign all of these modes, the polarization ratio measurement and different excitations are relevant. For example, the most strongly enhanced band at 1380 cm^{-1} via 457.9 nm excitation has the polarized character, thus this band is assignable as ν_4. Since 1370 and 1364 cm^{-1} bands have different polarization and enhancement patterns depending on the excitation wavelength, these bands are ascribed to ν_{41}(B) and ν_{41}(A), respectively. The 1355 cm^{-1} band has depolarized band character, and there is no corresponding peak in the IR spectrum. Probably it is reasonable that this band is due to the ν_{13} mode contribution. The 1349 cm^{-1} band is a B-phenyl mode in analogy with the IR spectrum. The other small bands are tabulated in Table 3.

For ZnTPP, the similar features are found except some alterations in the intensity pattern (Figure 8). The A-phenyl

mode is not strongly enhanced even though this band is very strong in the IR spectrum. However, the other phenyl modes are observed which are due to C- and F-phenyl mode contributions, respectively. The anomalously polarized band at 1556 cm^{-1} can be assigned as ν_{20} which was not found in the previous studies, because this mode is enhanced via Q band excitation and the strong fluorescence swamps out the RR spectra (Figure 8, spectrum via 514.5 nm excitation). Due to the liquid nitrogen temperature, a relatively good quality spectrum is obtained in our case. The strong bands at 1547 and 1353 cm^{-1} are polarized and consequently assigned as ν_2 and ν_4 modes, respectively. Interestingly, the ν_{13} mode at 1355 cm^{-1} is observed, which is not found in RR spectra of NiTPP. The other bands are tabulated in Table 4. For ZnTPC, as expected, the E$_u$ modes are split into A and B modes which are also Raman active and this behavior is more prominent compared to NiTPC (Figure 9). For example, ν_{38}, ν_{39}, ν_{40}, ν_{41} and ν_{44} modes can be found by pairs and assigned on the basis of the polarization ratio between A and B groups (Table 4). However the possibility of mixing with other modes can not be excluded, especially, for the ν_{39}(B) mode where ν_2 mode is normally observed at the same position.[18] A-, C-, E-. F-phenyl modes are observed at 1597, 1239, 1034 and 1004 cm^{-1} even though the A-phenyl mode is very weak

Comparative Vibrational Spectroscopic Studies

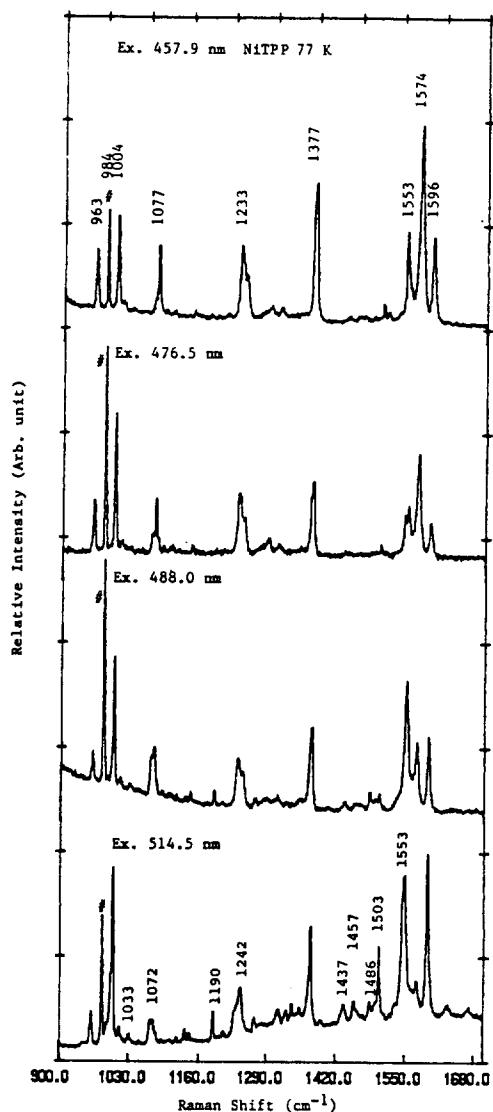Bull. Korean Chem. Soc., Vol. 10, No. 1, 1989 45

Figure 6. RR spectra of NiTPP pellet at 77 K via several excitation wavelengths and the internal standard peak is denoted by # mark, Conditions; 50 mW powder for each spectrum, slitwidth 4 cm^{-1} resolution, scan rate 1 cm^{-1}/sec.

Figure 7. RR spectra of NiTPC pellet at 77 K. The The other conditions are the same as in Figure 6.

in the Raman spectrum relative to the strong A-phenyl mode, which is enhanced strongly in the NiTPP RR spectrum (Figure 9 and Table 4). Generally the appearance of the phenyl modes in the TPP RR spectra has been ascribed to a mutual interaction between the phenyl group and the porphyrin excited state.[27] Thus the similar phenyl mode enhancement in TPC RR spectra suggests that a similar interaction is preserved in TPC. The general spectral features of NiTPC and ZnTPC shown here are the result of the effective molecular symmetry lowering. The polarized ν_2 mode is observed at 1546 cm^{-1}. As already observed in NiTPC, from 1340 to 1400 cm^{-1} region four relatively strong bands are enhanced with alterations in intensities depending on the excitation wavelengths and different polarization characters. From these observations, 1354 cm^{-1} band could arise from ν_4 mode origin which is normally the most strongly enhanced via Soret band excitation and 1340 cm^{-1} band can be assigned as ν_{41}(dp) because of its depolarized behavior. The other small bands are tabulated in Table 4.
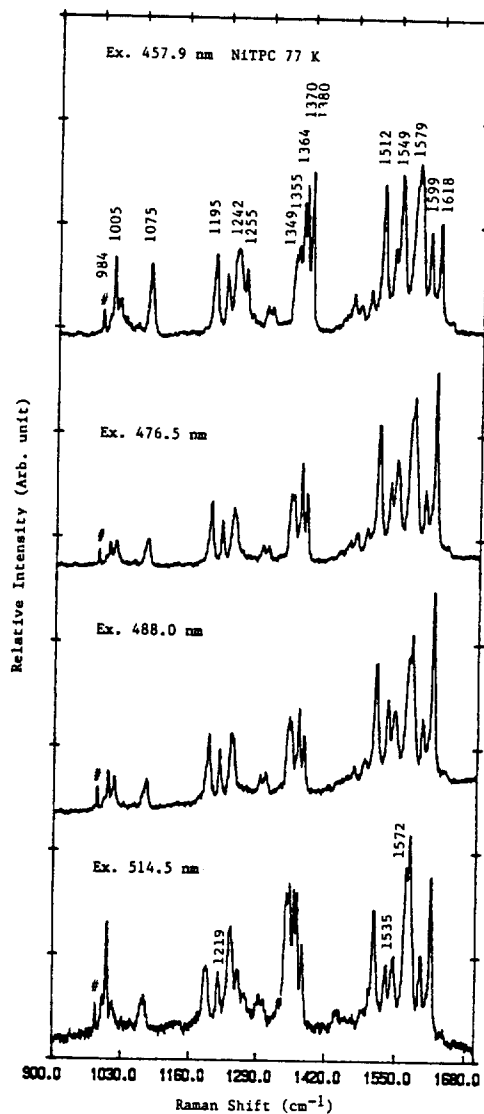
From the results of efforts in trying to extract the relationship between the structure of the metalloporphyrin and the Raman frequencies, the emprical correlation between the core size and Raman frequencies have been established.[26,28] The inverse linear relationship with the core-size has been attributed to a dependence of the force constant for the methine bridge bonds on the methine angle, the slopes of the correlation varying roughly with the contribution of the methine bond stretching to the normal modes.[26] For metallo TPP anologs, the core-size correlationship with high-frequency Raman bands at $\nu_3(A_{1g})$, $\nu_{20}(A_{2g})$ and $\nu_2(A_{1g})$ were found from the previous study. However, in recent studies this correlation has been extended to all high-frequency Raman modes above ν_4. According to the core-size correlationship equation $\nu = K(A-d)$ cm^{-1} where $d = C_f N$ (A) (metal to pyrrole nitrogen distance), for metallo-TPP's it was observed that the values of the parameters are in the same range among TPP and PP (protoporphyrin) and there is a rough parallelism in the order of increasing K, with ν_4 having the lowest value in each case.[26] For ν_4, ν_2 and ν_{10} the values of K are actually quite similar, but for the remaining modes they differ

Figure 8. RR spectra of ZnTPP pellet at 77 K. The other conditions are the same as in Figure 6.
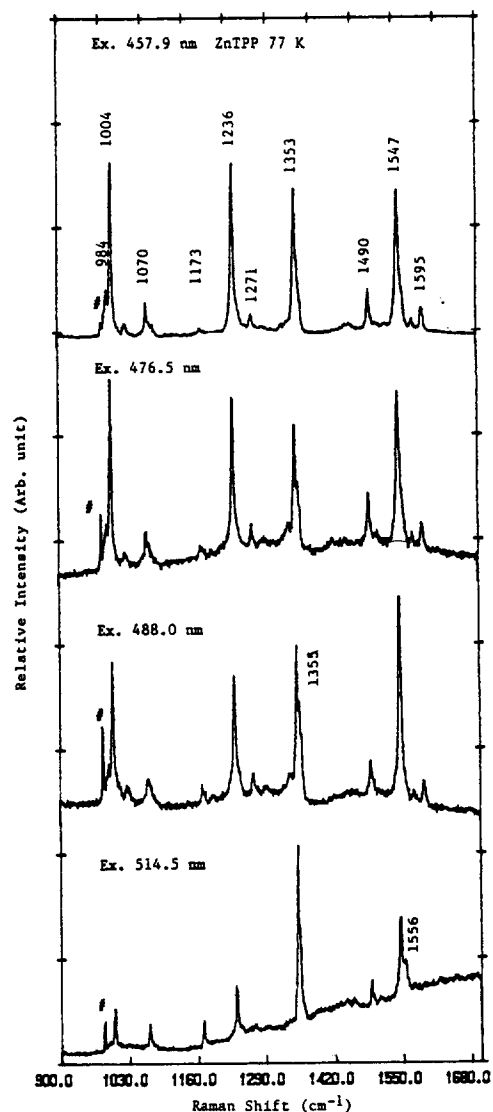

Figure 9. RR spectra of ZnTPC pellet at 77 K. The other conditions are the same as in Figure 6.

substantially between PP and TPP.[26] These differences no doubtfully reflect appreciable alterations in the normal mode compositions brought about by the differing substituent. From the previous X-ray crystallographic study, the core sizes for NiTPP and ZnTPP are 1.958 and 2.037 A, respectively.[22] Even though it might be expected that the core size for the chlorin is contracted relative to the porphyrin due to the saturation on C_b-C_b bond, it is assumed that the actual core size for the chlorin is similar to the porphyrin (at least the general trend might be similar) due to the lack of X-ray crystallographic data. The frequencies of the characteristic RR bands of ZnTPC is lower than those of NiTPC by 8~30 cm^{-1} depending on the modes for all the bands observed above 1350 cm^{-1} (Table 3 and 4) except ν_{41}(A) mode. However for the more thorough analysis, it is substantially necessary to accmulate vibrational frequency data on other metallo-TPC's. Tlhen it will be possible to evaluate whether the ruffled structure of the chlorin will cause the deviations in the core-size correlation or this relationship for the metalloporphyrin is generally applicable to the metallochlorin. An extended study on this subject is currently under
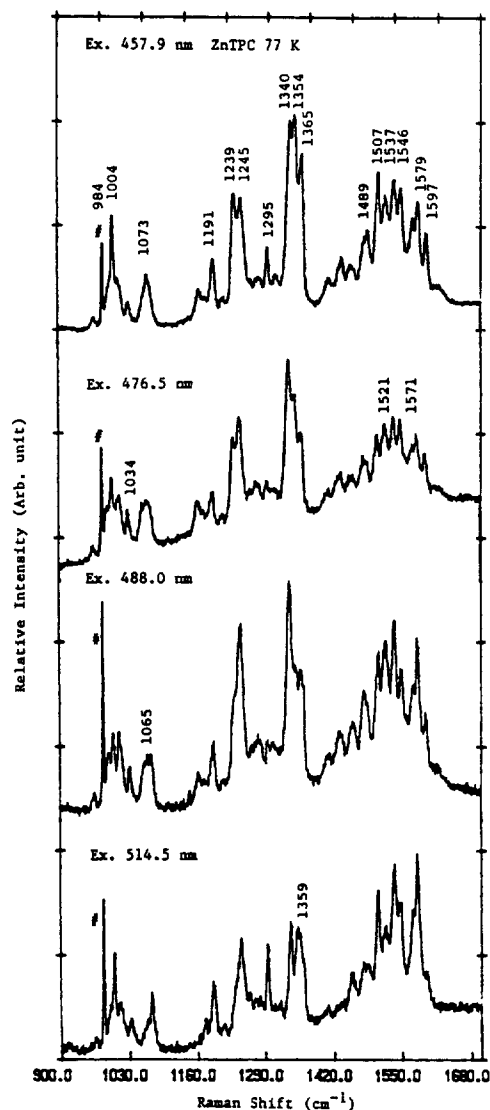
way.

Conclusion

From the results of our experiments, an attempt was made to assign the metallo-TPC modes combined with the polarization ratio measurement, the various excitation wavelengths and the comparision with metallo-TPP frequencies. The rough correlation between the metallo-TPC core-size and the Raman frequencies might exist. Generally like other metallochlorins, the RR and IR spectra are found to be more complex relative to the metalloporphyrin due to the splitting of E_u modes into A and B groups which are Raman active. The enhancement pattern is quite different due to the different substituents relative to the metalloporphyrin, however, the same vibrational parameters of other type of metallochlorins are applicable to metallo-TPC's.

References

1　(a) T. G. Spiro, *Adv. Protein cm.,* **37**, 111 (1985); (b) T Kitagawa and Y. Ozaki, *Struct. Bondings,* **64**, 71 (1987).

2. J. Barber, ed., Topics in photosynthesis, Vols. 1-3, Elsevior, Amsterdam (1979).

3. D. Dolphin, ed., The prophyrins, Vols. 1-7, Academic Press, New York (1978).

4. T. A. Walsh, M. K. Jonhson, D. Barber, A. J. Thomson and C. J. Greenwood, *Inorg. Biochem.,* **14**, 15 (1981).

5. T. Brittain, C. Greenwood and D. Barber, *Biochim. Biophys. Acta.,* **705**, 26 (1982).

6. L. A. Andersson, T. M. Loehr, A. R. Lim and A. G. Mauk, *J. Biol. Chem.,* **259**, 15340 (1984).

7. S. S. Sibbet and J. K. Hurst, *Biochem.,* **23**, 3007 (1984).

8. G. T. Babcock, R. T. Ingle, W. A. Oertling, J. C. Davis, B. A. Averill, C. L. Hulse, D. J. Stufkens, B. G. J. M. Bolscher and R. Wever, *Biochem. Biophys. Acta.,* **828**, 58 (1985).

9. M. Lutz, In Advances in Infrared and Raman Spectroscopy, Vol. 11, pp 211-300, R. J. H. Clark and R. E. Hester Eds; Wiley-Heyden, London (1984).

10. R. K. Poole, B. S. Baines, J. A. M. Hubbard, M. N. Hughes and N. J. Campell, *FEBS Lett.,* **150**, 147 (1982).

11. T. M. Cotton, R. Timkovich and M. S. Cork, *FEBS Lett.,* **133**, 39 (1981).

12. Y. Ching, M. R. Ondrias, D. L. Rousseau, B. B. Muhoberac and D. C. Wharton, *FEBS Lett.,* **138**, 239 (1982).

13. Abbreviations used here; Mi; Metal, OEC; Octaethylchlorin, TMC; Tetramethylchlorin, TPC; Tetraphenylchlorin, TPP; Tetraphenylporphyrin, PP; Protoporphyrin.

14. L. K. Hanson, C. K. Chang, B. Ward, P. M. Callahan, G. T. Babcock and J. D. Head, *J. Am. Chem. Soc.,* **106**, 3950 (1984).

15. L. A. Andersson, T. M. Loehr, C. K. Chang and A. G.

16. Mauk, *ibid,* **107**, 182 (1985).

16. (a) Y. Ozaki, T. Kitagawa and H. Ogoshi, Inorg. Chem. **18**, 772 (1979); (b) Y. Ozaki, K. Iriyama, H. Ogoshi, T. Ochiai and T. Kitagawa, *J. Phys. Chem.,* **90**, 6105 (1986); (c) Y. Ozaki, K. Iriyama, H. Ogoshi, T. Qchiai and T. Kitagawa, *ibid,* **90**, 6113 (1986).

17. (a) L. A. Andersson, T. M. Loehr, C. Sotirion, W. Wu and C. K. Chang, *J. Am. Chem. Soc.,* **108**, 2908 (1986); (b) L. A. Andersson, C. Sotirion, C. K. Chang and T. M. Loehr, *ibid,* **109**, 258 (1987).

18. (a) N. J. Boldt, R. J. Donohoe, R. R. Birge and D. F. Bocian, *J. Am. Chem. Soc.,* **109**, 2294 (1987); (b) N. J. Boldt and D. F. Bocian, *J. Phys. Chem.,* **92**, 581 (1988); (c) P. Hilderbrandt and T. G. Spiro, *ibid,* **92**, 3355 (1988).

19. H. W. Whitlock, R. Hanauer, M. Y. Oester and B. K. Bower, *J. Am. Chem. Soc.,* **91**, 7485 (1969).

20. J. Fajer, D. C. Borg, A. Forman, R. H. Felton, L. Vegh and D. Dolphin. N. Y. Acad. *Sci.,* **206**, 349 (1973).

21. J. C. Seo, Y. B. Chung and D. Kim, App. Spectrosco. **41**, 1199 (1987) .

22. J. L. Hoard, In Porphyrins and Metalloporphyrins, Chapter 8, ed. K. M. Smith, Elsevior. Amsterdam, (1975).

23. J. C. Gallucci, P. N. Swepston and J. A. Ibers, Acta. Crystallogr. Sect B, B38, 2134 (1982).

24. L. D. Spaulding, L. C. Andrews and G. J. B. Williams, *J. Am. Chem. Soc.,* **99**, 6918 (1977).

25. S. H. Strauss, M. E. Silver, K. M. Long, R. G. Thompson, R. A. Hudgens, K. Spartalian and J. A. Ibers, *J. Am. Chem. Soc.,* **107**, 4207 (1985).

26. N. Parthasarathi, C. Hansen, S. Yamaguchi and T. G. Spiro, *J. Am. Chem. Soc.,* **109**, 3865 (1987).

27. J. M. Burke, J. R. Kincaid and T. G. Spiro, *J. Am. Chem. Soc.,* **100**, 6077 (1978).

28. P. Stein A. Ulman and T. G. Spiro, *J. Phys. Chem.* **88**, 369 (1984).

Solvolysis of Phenylacetyl Chlorides in Methanol-Acetonitrile Mixtures

Ikchoon Lee*, Chul Huh, and Hai Whang Lee

Department of Chemistry, Inha University, Inchon 402-751. Received August 10, 1988

The methanolysis reactions of phenylacetyl chlorides have been investigated in methanol-acetonitrile mixtures at temperatures ranging $-15.0-0.0$ °C. Substituent and solvent effects on the rate supported an associative S_N2 mechanism for the solvolysis. Activation parameters indicated that the reaction is entropy controlled, while the a/s ratios of the Taft's solvactochromic correlation proved to be remarkably constant with a typical value of 0.50 that is consistent for the reactions proceeding by a typical S_N2 path.

Introduction

The reactions of acyl chlorides, RCOCl, have been studied extensively partly because they are the most widely used reactions in organic synthesis[1]. However due to their strong reactivity, the mechanisms are not well elucidated compared to the mechanisms of reactions of other carbonyl compounds. To remedy the situation, various experimental devices for the fast-rate measurement have been introduced[2].

Ethanolysis of aliphatic acyl chlorides[3] are reported to proceed by a bimolecular synchronous displacement (S_N2)